Asian Journal of Chemistry; Vol. 26, No. 18 (2014), 6279-6284

ASIAN JOURNAL OF CHEMISTRY

http://dx.doi.org/10.14233/ajchem.2014.17660

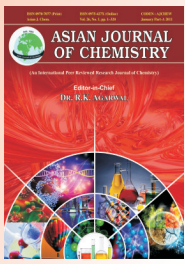

Synthesis of Amorphous MnO_2/MWCNT Nanocomposites and Their Electrochemical Properties

JIE HU[1,2,*], LINA SHI[1], JIE MEN[1] and LINA WANG[1]

[1]Hebei Key Laboratory of Applied Chemistry, Department of Environment and Chemistry, Yanshan University, Qinhuangdao, 066004, P.R. China
[2]State Key Laboratory of Metastable Materials Science and Technology, Yanshan University, Qinhuangdao 066004, P.R. China

*Corresponding author: E-mail: hujie@ysu.edu.cn

Received: 25 March 2014; *Accepted*: 27 May 2014; *Published online*: 1 September 2014; AJC-15899

MnO_2/MWCNT nanocomposites has been fabricated through a simple route in a water-reflux condenser system under different temperature. The as-prepared composites were characterized by scanning electron microscopy, transmission electron microscopy, X-ray diffraction and Brunauer-Emmett-Teller surface area analysis. Capacitive properties of the synthesized composite electrodes were investigated *via* cyclic voltammetry, galvanostatic charge/discharge and electrochemical impedance spectrometry in a 0.5 M Na_2SO_4 electrolyte. Results show that this method can control the number and size of MnO_2 particles loaded onto the surface of MWCNTs. Because excessive MnO_2 enwrapping carbon nanotubes would affect the overall conductivity, the composite prepared by lower temperature has better characteristics of super capacitor. 60-MnO_2/MWCNT composite (51 wt. % MnO_2) displays the specific capacitance as high as 337 F/g at 1000 mA/g, which is higher than that of 100-MnO_2/MWCNT (290 F/g) and exhibited an excellent cycling stability with no more than 6 % capacitance loss after 1000 cycles.

Keywords: MWCNTs, MnO_2, Composite, Supercapacitor.

INTRODUCTION

Recently, supercapacitors have attracted intensive research interest due to their capability to deliver high power density, which makes them indispensable candidates as power boosters for hybrid electric vehicles, mobile electronic devices, distributed sensor networks and so on[1]. Various transition metal oxides have been investigated as electrode materials. Among them, MnO_2 is intensively exploited as one of the most promising electrode materials due to its high theoretical capacity, favorable pseudocapacitive behaviour, environmental benign nature, natural abundance and low cost[2]. Nevertheless, a major drawback of MnO_2 is its poor electrical conductivity, which limits its power-delivery capability. An effective approach to overcome this disadvantage is the introduction of electronically conductive materials (*e.g.*, carbon black and CNTs). Because of this, various MnO_2/CNTs nanocomposites have been studied.

Subramanian *et al.*[3] prepared MnO_2/SWNT composites with different SWNT contents by adding ethanol as the reducing agent to the $KMnO_4$ solution with dispersed single wall carbon nanotubes. Jiang *et al.*[4] carry out a similar experiment uses multi wall carbon nanotubes as carrier. Danilov & Melezhyk[5] and Ko *et al.*[6] also prepared MnO_2/CNT composite separately using formic acid, acetic acid and manganese as reducing agent. Fan *et al.*[7] oxidized $MnSO_4$ by using $(NH_4)_2S_2O_4$ and $(NH_4)_2S_2O_8$ and assisted by microwave, prepared MnO_2 nano sheet by CNT as skeleton. Teng *et al.*[1,2] prepared MnO_2/CNT composite materials with different morphology by hydrothermal method with $MnSO_4$ as the precursor, $KMnO_4$ and $(NH_4)_2S_2O_8$ as oxidant, respectively. Fan *et al.*[8] loaded MnO_2 to graphite electrode which was modified by carbon nanotubes with using thermal decomposition nitrate. Xie and Gao[9] prepared MnO_2/CNT composite capacitor material with carbon nanotubes as reducing agent to deoxidize $KMnO_4$. Many students[10-16] synthesized some different morphological MnO_2/CNT composite material with better performance on the basis, by adjusting the synthesis conditions, introducing ultrasonic, microwave method and other means.

In the process of fabricating electrodes, the choices of the current collectors and methods of depositing activated materials on them are the most crucial element to affect the performance of ECs. As one of the most economical and versatile methods for depositing and coatings, electrophoretic deposition (EPD) enables the formation of high purity deposits of uniform thickness on substrates with complex shape.

In this paper, we reported a facile method to prepare MnO_2/MWCNT nanocomposites as novel electrode materials through a simple route in a water-reflux condenser system under different tempreture and fabricating electrodes by using electrophoretic deposition. The schematic illustration of the structure of this

hybrid material is shown in Fig. 2. Uniform nano-scaled MnO_2 coatings on MWCNT could improve the utilization of MnO_2 and the electrical conductivity of electrode with presence of the MWCNT. The microstructure of the MnO_2/MWCNT hybrid sample was revealed by field-emission electron microscopy (FE-SEM), high-resolution transmission electron microscopy (HRTEM) and X-ray diffractometry (XRD).The capacitive behaviours of the MnO_2/MWCNT nanocomposites under different tempreture were investigated and compared with that of the MnO_2 electrode in 0.5 M Na_2SO_4 electrolyte solution.

EXPERIMENTAL

Synthesis of MnO_2/MWCNT composites: The MWCNTs prepared by chemical vapor deposition were purchased from Shenzhen Nanotech Port Limited Company. Their outer diameter and length were 80-90 nm and 20-30 μm on average. MnO_2 were prepared by redox reaction between acetylene black and potassium permanganate under a traditional chemical precipitation method. With MWCNTs as carrier, the MnO_2 particles showed nucleation and growth. Fig. 1 shows the schematic diagram of MnO_2/MWCNT composites. In the first step, 100 mL of MWCNTs (without any pretreatment) water suspension (2.7 mg/mL) was subjected to ultrasonic vibration for 1 h. Then $KMnO_4$ powder (0.5 g) and acetylene black (0.03 g) were added into above MWCNTs suspension. Subsequently, the aqueous suspension was reflux condensed in a thermostatic water bath by constant magnetic stirring at the temperature of 60 and 100 °C for 6 h, respectively. Finally, the black deposit was filtered, washed several times with distilled water and alcohol and dried at 70 °C for 12 h in a vacuum oven. The sample collected after dried is designated as X-MnO_2/MWCNT, where X denoted the synthesis temperature. For comparison, the pure MnO_2 was prepared at 60 °C under the same condition.

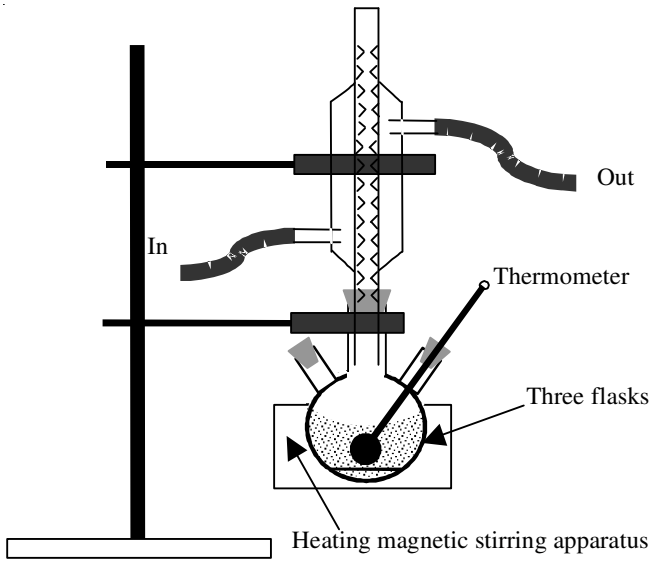

Fig. 1. Synthesis schematic diagram of amorphous MnO_2/MWCNT nanocomposites

The resulting mass percentages of MnO_2 in the composites were determined by inductively coupled plasma-atomic emission spectroscopy (ICP-AES, Shimadzu ICPS-7500). Furthermore, in order to examine the mass percentage of MnO_2 in the MnO_2/MWCNT composites, thermogravimetry (TG)-differential scanning calorimetry (DSC) experiments (STA 449C, NETZSCH, SELB, Germany) were carried out.The crystallographic structures of the materials were determined by X-ray diffraction (XRD, D/max -2500/pc) with CuK_α radiation λ = 1.5405 Å. The Brunauer-Emmett-Teller (BET) specific surface areas were evaluated based on nitrogen adsorption isotherms at -196 °C on a NOVE 4000e analyzer. The microstructure of the samples was investigated by a field-emission scanning electron microscopy (FESEM, S-4800) and a transition electron microscopy (TEM, JEOL JEM2010).

Preparation of electrodes and electrochemical measurement: The fabrication of working electrodes is shown in Fig. 2. The aqueous suspension of composites with a concentration of 1 g/L was used for the electrophoretic deposition. The nickel foam substrates (1 cm × 1 cm) were cleaned by ultrasonic treatment in ethanol for 0.5 h and drying under vacuum at room temperature. Two parallel nickel foams were used as electrodes at a distance of 1 cm. Electrophoretic deposition was conducted at a constant voltage of 10 V for a deposition time of 10 min. After deposition, the samples were dried under vacuum at room temperature. The loading mass of each electrode was about 2 mg.

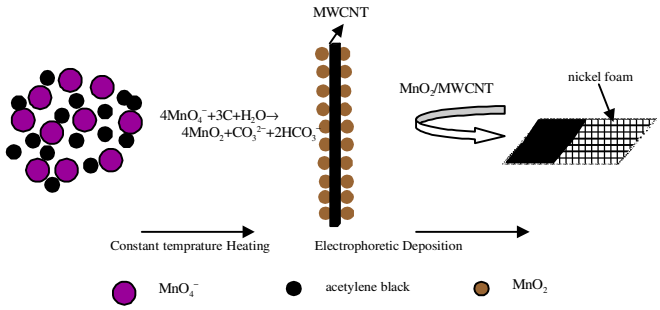

Fig. 2. Procedure for the fabrication of the MnO_2/MWCNT electrode

The electrochemical measurements were performed in a three-electrode system with a nickel foam (3 cm × 3 cm) electrode and a saturated calomel electrode (SCE) served as counter and reference electrodes respectively. The prepared Ni foam coated with composites, only an area of 1 cm × 1 cm was exposed for electrochemical measurement as the working electrode. The measurements were carried out in a 0.5 M Na_2SO_4 aqueous electrolyte at room temperature. Galvanostatic charge/discharge curves were measured in the potential range of 0-1.0 V at current densities of 1000 mA/g. Cyclic voltammograms tests were carried out at potentials between -0.2 and 1 V at scan rates of 20 mV/s. Electrochemical Impedance spectroscopy were carried out without DC bias sinusoidal signal of 5 mV over the frequency range from 10 kHz to 0.1 Hz.

RESULTS AND DISCUSSION

Microstructure characterizations: A relatively easier method was adopted to estimate the mass percentage of MnO_2 in the MnO_2/MWCNT. Fig. 3 shows thermogravimetry and differential scanning calorimetry curves of MWCNT and 60-MnO_2/MWCNT. About from 600 °C, the MWCNT sample burned up and completely at approximately 743 °C with a

residual mass of 1.6 %, which have some residual impurities. The differential scanning calorimetry curve of MnO_2/MWCNT showed a slow weightlessness before 350 °C because of the evaporation of free water and the lost process of crystal water, then the followed weight loss originated from the oxidation of MWCNT. At the temperature about 750 °C, MnO_2 was reduced to Mn_2O_3, so a smaller endothermic peak appeared. A similar reduction of Mn^{4+} to Mn^{3+} and loss of structural O anions has been reported for MnO_2[17]. It can be seen from thermogravimetry curve of MnO_2/MWCNT, at the temperature up to 800 °C, the residual mass was about 49.4 %. Therefore, the mass percentage of MnO_2 in the MnO_2/MWCNT was estimated to be 51 %. The mass percentage of MnO_2 in the MnO_2/MWCNT was also determined by using ICP-AES, it correlates well to the thermogravimetry/differential scanning calorimetry experiments.

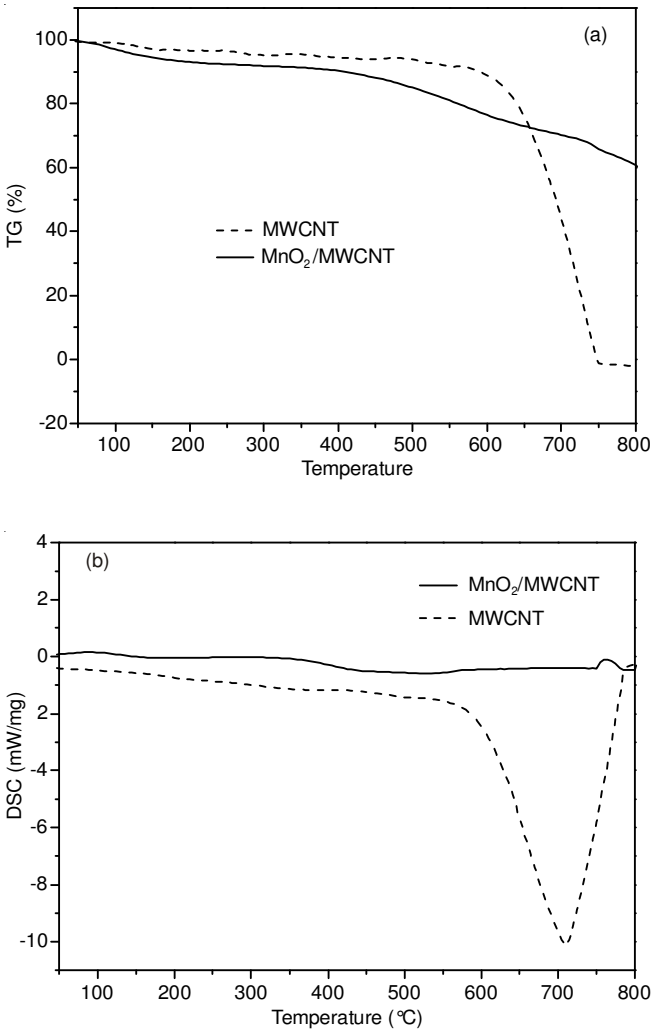

Fig. 3. thermogravimetry (a) and differential scanning calorimetry (b) curves of MWCNT and 60-MnO_2/MWCNT

Fig. 4 shows the typical XRD patterns of the as-prepared 60-MnO_2/MWCNT and 100-MnO_2/MWCNT samples, which can provide more information of the sample was further performed to characterize the structure of the MnO_2/MWCNT. XRD analysis confirms the presence of the three broad peaks at 2θ around 24.8°, 36.8° and 66.3° can be indexed to birnessite-type MnO_2 (JCPDS 42-1317)[18] with mixed crystalline and amorphous parts. Besides the MWCNT peaks, there were only very weak and broad peaks about MnO_2 in the pattern of 60-MnO_2/MWCNT, suggesting a small number of poorly crystallized nanocrystals in the amorphous MnO_2 compound. While, the MnO_2/MWCNT nanocomposites were prepared at 100 °C had better crystallinity. It indicates that resultant temperatures play an important role on preparing MnO_2/MWCNT nanocomposites by using water-reflux condenser system, which can control the growth degree of MnO_2 in MWCNT.

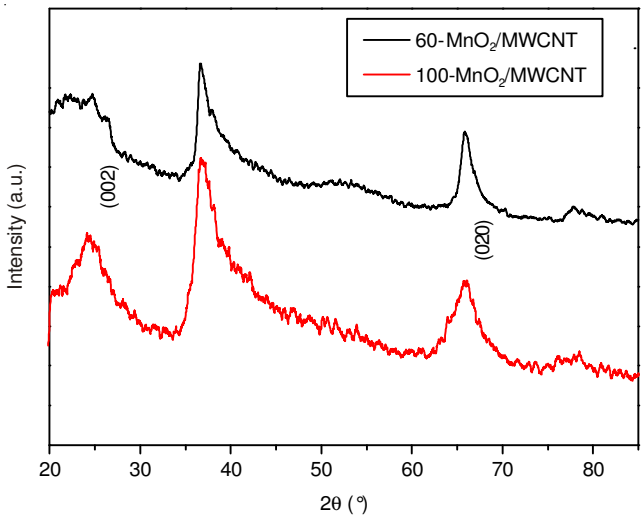

Fig. 4. XRD pattern of 60-MnO_2/MWCNT and 100-MnO_2/MWCNT

Fig. 5 displays the nitrogen adsorption-desorption isotherms and pore size distribution curves calculated by BJH method. In the low relative pressure ($P/P_0 < 0.4$), the adsorption and desorption curves coincide because there is monolayer adsorption and reversible phenomena. At the higher relative pressure region (P/P_0 0.4-0.85), the isotherms all have significant hysteresis, indicating their mesoporous characteristics[19]. The specific surface area for each sample was obtained by BET method and the value for MnO_2, 60-MnO_2/MWCNT and 100-MnO_2/MWCNT were 243.1, 347.8 and 316.9 m^2/g, respectively. BJH analysis for mesopore distribution is shown in Fig. 5b, the pore volumes for 60-MnO_2/MWCNT and 100-MnO_2/MWCNT are respectively 0.41 and 0.34 mL/g. It can be seen from Fig. 5b, the pore size distribution of 60-MnO_2/MWCNT is wider than 100-MnO_2/MWCNT. The pore size of the 100-MnO_2/MWCNT sample is mainly center around 4 nm and the 60-MnO_2/MWCNT is in range of the 2-5 nm. It is well known that the uniform pore sizes in the range of 3-5 nm are required to improve the capacitance in EDLCs[20]. The pore structure of MnO_2 particles is the main channel of electrolyte penetration, the rich mesoporous are good for the full contact between materials surface and electrolyte surface and improve the utilization rate of materials.

The microstructure images of MnO_2/MWCNT composites are shown in Fig. 6. When the resultant temperature is 60 °C, it can be seen from Fig. 6a that some MnO_2 nanoparticles had been directly deposited on the surface of the MWCNT, showing the MWCNT were partly decorated. After the redox reaction between acetylene black and $KMnO_4$ through a water-reflux

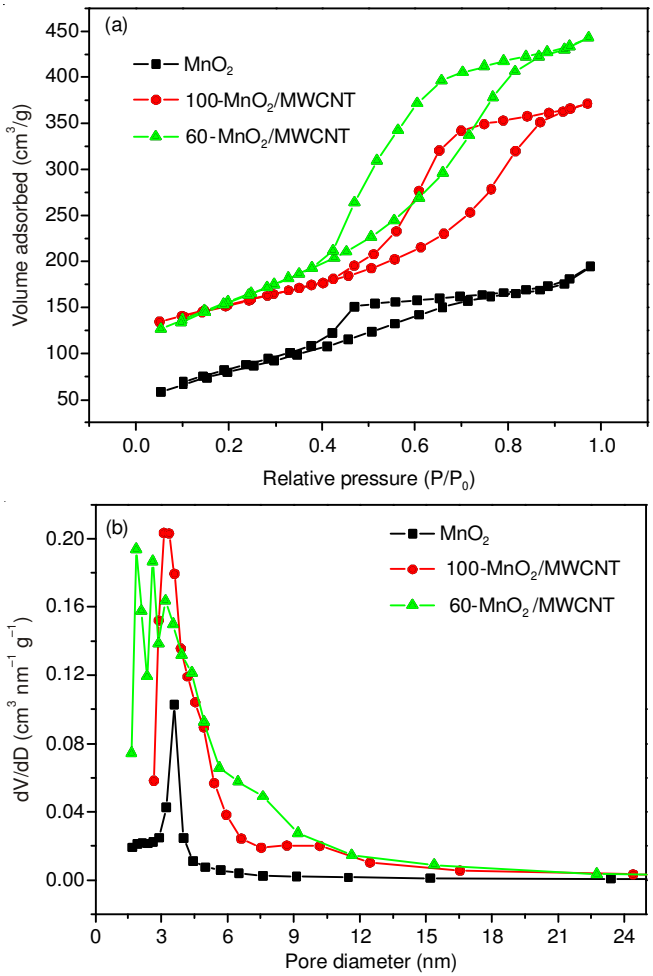

Fig. 5. N_2 adsorption-desorption isotherms (a); Pore size distributions calculated by BJH (b)

condenser system (Fig. 1) under 100 °C resultant temperature, as can be seen from Fig. 6b, the MWCNT were completely decorated homogeneously with MnO_2 nanopar-ticles.

Fig. 6(c) and Fig. 6(d) show the TEM and HRTEM images of 60-MnO_2/MWCNT. The MnO_2 exhibits the same interlayer spacing, 0.72 nm, corresponding to (002) crystal planes, indicating that there was no change in the lattice structure of MnO_2 after MWCNT was introduced. Under the 60 °C constant temperature conditions, the redox reaction between acetylene black and $KMnO_4$ may take place on the MWCNT surface. Therefore, MnO_2 can grow on the MWCNT surface. As can be seen from the TEM images, acetylene black as a reducing agent, which instead of the ectotheca of MWCNT to react with $KMnO_4$, so it offers some degree of protection to the morphology and structure of original MWCNT. Compared with Fig. 6(b), it can be seen from Fig. 6(a) that 60-MnO_2/MWCNT have wider pore size distribution. The highly porous structure can shorten the diffusion path for charge-carrier ions, while the large liquid-solid interface facilitates ion exchange between the electrode and electrolyte. Moreover, the uniformly embedded electronic conducting network can improve the high-rate capability as well as the specific capacitance of the materials. Furthermore, excessive MnO_2 on MWCNT wrapped will affect its overall conductivity. Therefore the composite prepared at 60 °C constant temperature method has better the super capacitor.

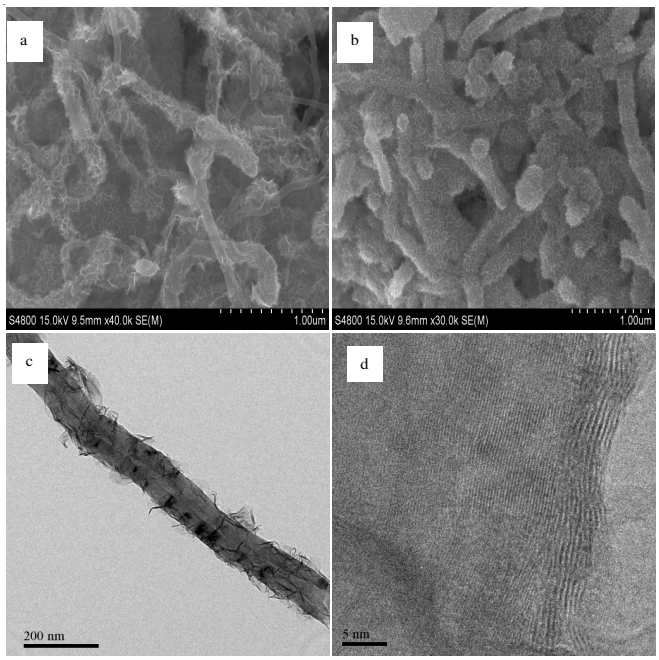

Fig. 6. SEM images of 60-MnO_2/MWCNT (a) and 100-MnO_2/MWCNT (b), TEM (c) and HRTEM (d) images of 60-MnO_2/MWCNT

Electrochemical behaviour: The cyclo voltammogram curves of MnO_2, 60-MnO_2/MWCNT and 100-MnO_2/MWCNT at a 20 mV/s scan rate in 0.5M Na_2SO_4 aqueous solution are shown in Fig. 7a. It is clear that all of the cyclo voltammogram curves are almost ideally rectangular, exhibiting the typical electrochemical double-layer capacitive behaviour with a rapid current response on voltage reversal at each end potential and high reversibility. Obviously, 60-MnO_2/MWCNT and 100-MnO_2/MWCNT show higher integrated area than MnO_2 electrode, which indicates that the excellent electrochemical performance. The lack of symmetry in MnO_2/MWCNT is probably due to combined double-layer and pseudocapacitive contribution to the total capacitance.

The cyclic stability of MnO_2, 60-MnO_2/MWCNT and 100-MnO_2/MWCNT electrodes were also evaluated by CV test at a 20 mV/s scan rate for 1000 cycles. As shown in Fig. 7b, the capacitance of the electrode after 1000 cycle is smaller than that of the first cycle, which may be ascribed to the loose of the active materials in electrode or the mass losing of the electrode after 1000 times of cycle. The capacitance of 60-MnO_2/MWCNT electrodes decreases by 6.1 % than the initial capacitance after 1000 cycles, demonstrating excellent electrochemical stability of such electrode material.

EIS measurements were generally applied to evaluate the electrochemical properties of the as-prepared electrode samples. Typical Nyquist plots of EIS for these electrodes are displayed in Fig. 7c. All the impedance plots are composed of a semicircle in the high frequency range and a straight line in the low frequency range. The measured impedance spectra were analyzed on the basis of the equivalent circuit, which is given in the inset of Fig. 7c. At high frequencies, the intercept at real part (Z') is a combinational resistance of ionic resistance of electrolyte, intrinsic resistance of substrate and contact resistance at the active material/current collector interface. It can be seen from Fig. 7c, a major difference is the semicircle,

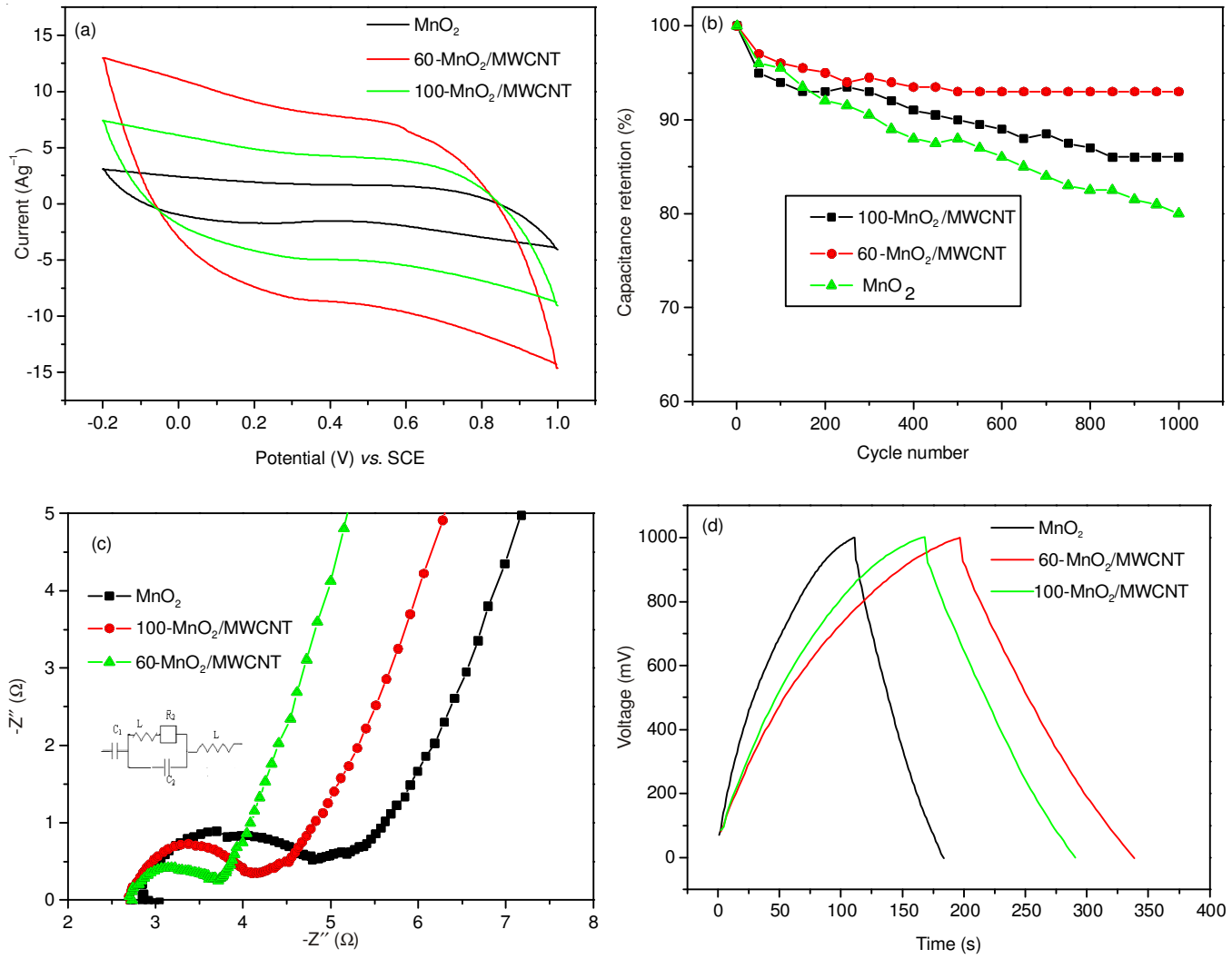

Fig. 7. (a) Cyclo voltammogram curves at 20 mV/s, (b) cycle life at 1 A/g, (c) Nyquist plots of electrodes, inset is the electrical equivalent circuit used for fitting impedance spectra, (d) Galvanostatic charge/discharge curves of MnO_2 (60- and 100-MnO_2/MWCNT at 1 A/g in 0.5 M Na_2SO_4 solution)

which corresponds to the charge transfer resistance (R_{ct}) caused by the Faradaic reactions and the double-layer capacitance on the grain surface. Comparing the impedance plots of these electrodes, it is apparent that the values of R_{ct} gradually decrease with introducing MWCNT and lower synthesis temperature. The straight line with the slope of 45 °C in the low frequency range is related to the diffusive resistance of the electrolyte into the interior of the electrode and ion diffusion into the electrode.

To get more information about the potential of as synthesized MnO_2/MWCNT nanocomposites as electrode materials for supercapacitors, galvanostatic charge/discharge measurements were carried out. As illustrated in Fig. 7d, during the charging and discharging steps, the charge curves are almost symmetric to its corresponding discharge counterpart with a slight curvature, indicating the pseudocapacitive contribution along with the double layer contribution. The specific capacitances (Cs) is calculated according to $Cs = I \times \Delta t/(m \times \Delta V)$ from the discharge curves, where I is the constant discharge current, Δt is the discharge time and ΔV is the potential drop during discharge and m (g) is the mass of active electrode material. The Cs values of MnO_2, 60-MnO_2/MWCNT and 100-MnO_2/MWCNT electrodes are 163, 337 and 290 F/g, respectively.

It is well known that the power characteristics of an electrode material strongly depend on the electrochemical kinetics of the redox reaction. Compared with MnO_2, the excellent electrochemical performances of MnO_2/MWCNT composite are greatly improved because of two reasons. First, well-dispersed nanoscale MnO_2 particles on the MWCNT surfaces can greatly reduce the diffusion length of Na^+ during the charge/discharge process, improving the electrochemical utilization of MnO_2. Second, the highly conductive MWCNT cores not only offer electron transportation capability to the MnO_2 shell, but also act as a buffer to alleviate the volume expansion. Moreover, the MWCNT can provide additional sites for (C^+) storage, which leads to an enhanced reversible capacity for the electrode. When the synthetic temperature is higher, excessive MnO_2 complete cover the MWCNT surface, which reduced the charge conduction properties of the MWCNT, no longer shaped a continuous conducting network, but also leded to the pore structure changes inside composite, increased the diffusion resistance of electrolyte ions in the composite electrode. Therefore the 60-MnO_2/MWCNT has better super capacitor than that of 100-MnO_2/MWCNT.

Conclusion

MnO_2/MWCNT nanocomposites had been fabricated through a simple soft chemical route in a water-reflux condenser system under different tempreture and investigated their electrochemical properties as supercapacitors. The morphology and structure of MnO_2 nanoparticles on the surface of MWCNTs could be controled by adjusting the synthesis temperature, which is important for generating high electrochemical performances. The specific capacitance values of 60-MnO_2/MWCNT composite (51 wt. % MnO_2) electrode reached 337 F/g at 1000 mA/g and with about 94 % capacitance retention after 1000 times of charge/discharge cycle in 0.5 M Na_2SO_4 electrolyte, indicating a good application potential in supercapacitors as well as other power source systems.

ACKNOWLEDGEMENTS

The authors gratefully acknowledged the support of the National Natural Science Foundation of China (No. 51402253) and the Technology Support Program of Hebei Province (No. 13214411).

REFERENCES

1. F. Teng, S. Santhanagopalan, Y. Wang and D.D. Meng, *J. Alloys Comp*., **499**, 259 (2010).
2. F. Teng, S. Santhanagopalan and D.D. Meng, *Solid State Sci*., **12**, 1677 (2010).
3. V. Subramanian, H. Zhu and B. Wei, *Electrochem. Commun*., **8**, 827 (2006).
4. R. Jiang, T. Huang, Y. Tang, J. Liu, L. Xue, J. Zhuang and A. Yu, *Electrochim. Acta*, **54**, 7173 (2009).
5. M.O. Danilov and A.V. Melezhyk, *J. Power Sources*, **163**, 376 (2006).
6. J.M. Ko and K.M. Kim, *Mater. Chem. Phys*., **114**, 837 (2009).
7. Z.J. Fan, Z.W. Qie, T. Wei, J. Yan and S. Wang, *Mater. Lett*., **62**, 3345 (2008).
8. Z. Fan, J.H. Chen, M.Y. Wang, K. Cui, H. Zhou and Y. Kuang, *Diamond Rel. Mater.*, **15**, 1478 (2006).
9. X.F. Xie and L. Gao, *Carbon*, **45**, 2365 (2007).
10. S.B. Ma, K.W. Nam, W.S. Yoon, X.Q. Yang, K.Y. Ahn, K.H. Oh and K.B. Kim, *Electrochem. Commun*., **9**, 2807 (2007).
11. S.B. Ma, K.W. Nam, W.S. Yoon, X.Q. Yang, K.Y. Ahn, K.H. Oh and K.B. Kim, *J. Power Sources*, **178**, 483 (2008).
12. J. Yan, Z. Fan, T. Wei, J. Cheng, B. Shao, K. Wang, L. Song and M. Zhang, *J. Power Sources*, **194**, 1202 (2009).
13. M. Wang, C. Wang, G. Wang, W. Zhang and F. Bin, *Electroanalysis*, **22**, 1123 (2010).
14. H.Y. Chu, Q.Y. Lai, L. Wang, J.F. Lu and Y. Zhao, *Ionics*, **16**, 233 (2010).
15. H. Wang, C. Peng, F. Peng, H. Yu and J. Yang, *Mater. Sci. Eng. B*, **176**, 1073 (2011).
16. Z.J. Fan, M.M. Xie, X. Jin, J. Yan and T. Wei, *J. Electroanal. Chem*., **659**, 191 (2011).
17. J.H. Zhang, Y.H. Wang, J.B. Zang, G.X. Xin, Y.G. Yuan and X.H. Qu, *Carbon*, **50**, 5196 (2012).
18. S.B. Ma, K.Y. Ahn, E.S. Lee, K.H. Oh and K.B. Kim, *Carbon*, **45**, 375 (2007).
19. H. Zhou, S. Zhu, M. Hibino and I. Honma, *J. Power Sources*, **122**, 219 (2003).
20. K.H. An, W.S. Kim, Y.S. Park, Y.C. Choi, S.M. Lee, D.C. Chung, D.J. Bae, S.C. Lim and Y.H. Lee, *Adv. Mater*., **13**, 497 (2001).